Joule

CellPress

Article

Heat-Insulating Multifunctional Semitransparent Polymer Solar Cells

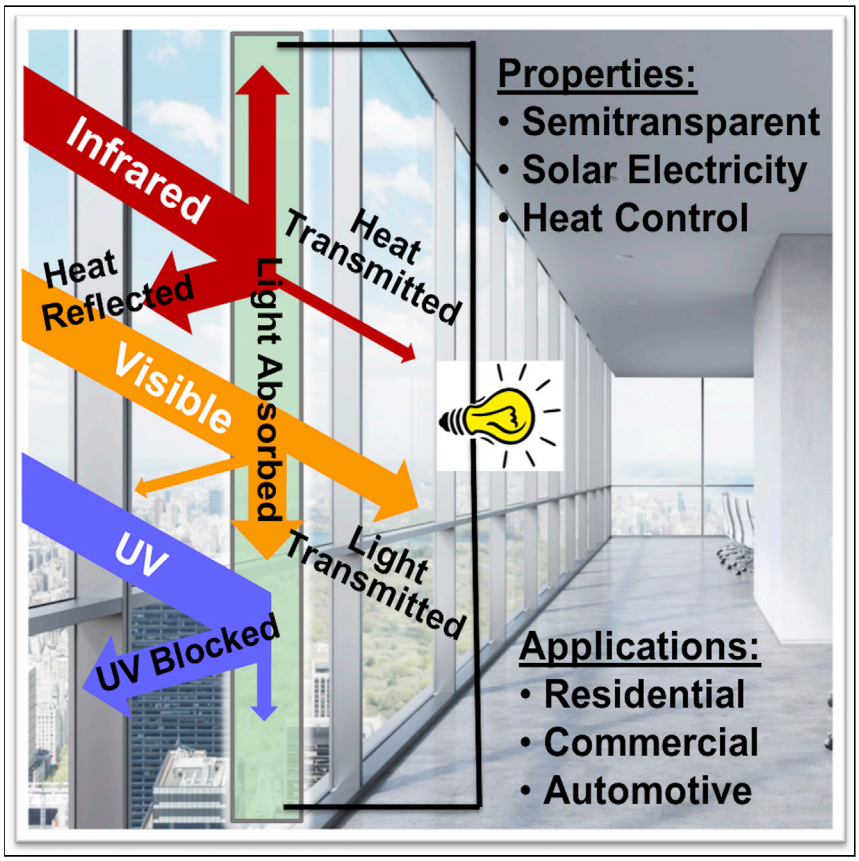

A dual-functional semitransparent organic photovoltaic cell that integrates both power-generation and heat-insulation functions is demonstrated. By introducing non-fullerene acceptor with enhanced near-infrared absorption and distributed Bragg reflectors for selectively keeping high reflectance for near-infrared light, the solar cell generates over 6% power conversion efficiency with high visible light transmission of over 25% in addition to an excellent infrared radiation rejection rate of over 80%.

Chen Sun, Ruoxi Xia, Hui Shi, ..., Fei Huang, Hin-Lap Yip, Yong Cao

msfhuang@scut.edu.cn (F.H.)
msangusyip@scut.edu.cn (H.-L.Y.)

HIGHLIGHTS

ST-OPVs can be simultaneously used for power-generation and heat-insulation films

Photonic structures are constructed to further enhance heat-insulating properties

Future design of multifunctional PVs for integration into daily life are proposed

Sun et al., Joule 2, 1–11
September 19, 2018
https://doi.org/10.1016/j.joule.2018.06.006

Please cite this article in press as: Sun et al., Heat-Insulating Multifunctional Semitransparent Polymer Solar Cells, Joule (2018), https://doi.org/10.1016/j.joule.2018.06.006

Joule

CellPress

Article

Heat-Insulating Multifunctional Semitransparent Polymer Solar Cells

Chen Sun,[1,4] Ruoxi Xia,[1,4] Hui Shi,[1] Huifeng Yao,[2] Xiang Liu,[1] Jianhui Hou,[2] Fei Huang,[1,*] Hin-Lap Yip,[1,3,5,*] and Yong Cao[1]

SUMMARY

Semitransparent organic photovoltaics (ST-OPVs) have attracted extensive attention due to their potential for integration into the windows of buildings. Herein, we propose a dual-functional ST-OPV device that is not only highly efficient but also very effective for heat insulation. By introducing non-fullerene acceptor with enhanced near-infrared absorption and distributed Bragg reflectors for selectively enhancing the transmittance in visible wavelengths while keeping high reflectance for near-infrared light, the ST-OPVs generate over 6% power conversion efficiency with high visible light transmission of over 25% and outstanding infrared radiation rejection rate of over 80%. Our results show that with proper design of ST-OPVs, they can be used not only for generating power from sunlight but also for solar shading and heat insulation, which opens up a new application of OPVs for both energy harvesting and saving.

INTRODUCTION

For widespread development of photovoltaics, it is critical to develop solar cells that are affordable for integration into standard products and systems. In this respect, the unique properties of being lightweight, mechanically flexible, solution processable, and compatible for large-scale manufacture make organic photovoltaics (OPVs) one of the most attractive photovoltaic technologies.[1–4] Semitransparent thin-film OPV cells have recently attracted growing attention in both the scientific and industrial communities due to their potential for use as power-generating windows in buildings, automobiles, or self-powered greenhouses.[5–7] In addition, the color tunability of conjugated organic semiconductors enabled by chemical and bandgap engineering allows different colors of solar cells to be manufactured to add esthetic value to architectural applications.

While semitransparent OPVs (ST-OPVs) have not yet been commercialized for power-generating window applications, commercial heat-control window films applied to the interior or exterior of glass windows to reduce the amount of UV, visible, and infrared (IR) light from sunlight are already widely used to improve energy efficiency of buildings.[8–10] These window films are usually coated with an extremely thin transparent metal (e.g., Ag or Al) film or other low-emissivity materials in order to reflect long-wave or significant amounts of short-wave IR energy.[11–13] This heat-insulation function can either be used to keep a room warm in winter or to reduce the room temperature in hot weather depending on the way the film is applied. With a more sophisticated optical design, such as the introduction of a distributed Bragg reflector (DBR) composed of multiple layers of alternating materials with varying refractive index, spectrally selective window films that can block out certain wavelengths of the sun's IR radiation and reject heat without reducing

Context & Scale

Commercial heat-control window films applied to the interior or exterior of glass windows to reduce the amount of UV, visible, and infrared light from sunlight are already widely used to improve energy efficiency of buildings, while semitransparent organic photovoltaics (ST-OPVs) have not yet been commercialized for power-generating window applications.

Here we have demonstrated for the first time that power-generation and heat-insulation functions can indeed be integrated together in specially designed ST-OPVs, which not only provide good power-generation properties but also show heat rejection comparable with that of commercial window films. A value-added ST-OPV with high PCE and AVT in addition to an excellent infrared radiation rejection rate have been demonstrated, which paves the way for the new application of OPV technology for both power generation and power saving.

natural visible light can be achieved.[14] Therefore, window films play an important role in the overall performance of a window and can significantly affect the overall heating, lighting, and cooling costs of a building.

ST-OPVs indeed can be designed with optical function very similar to that of commercial window films. With proper design of the ST-OPV device architecture, it can transmit a portion of visible light but also can absorb or reflect UV and IR photons to achieve UV protection and heat-rejection functions, although the latter properties have been rarely investigated. Currently the major parameters used to evaluate the overall performance of ST-OPVs are power conversion efficiency (PCE) and average visible transmittance (AVT).[15–17] Unfortunately these are usually competing parameters, and the challenge is to develop new materials and device engineering approaches to improve the overall performance of ST-OPVs by simultaneously achieving both high PCE and AVT.[18–20] A possible route to achieve this goal is to develop new small-bandgap materials with selective light-harvesting properties in the IR region while allowing most of the visible light to pass through. In earlier studies, small-bandgap donor polymers with a near-IR (NIR) absorption band have been successfully introduced to enhance NIR photon harvesting for polymer:fullerene-based ST-OPVs.[21,22] Recently, non-fullerene acceptors featuring improved absorption and low energy loss during the charge-generation process have been developed as the new generation of electron acceptors, enabling both opaque OPV and ST-OPV devices to reach record high efficiency.[23–27] The versatility of the molecular design of non-fullerene acceptors enables them to have facile tunable bandgaps and energy levels, providing powerful means to achieve broader IR light absorption as well as high open-circuit voltage (V_{oc}) that can lead to higher ST-OPV performance.[28–30]

In this study, we aim to integrate both the power-generation and heat-insulation functions for the first time to demonstrate a high-performance ST-OPV with heat-rejection properties comparable with those of commercial window films. A small-bandgap non-fullerene acceptor with absorption edge extended to 900 nm was chosen as the key component to harvest the NIR light in the bulk-heterojunction film.[31] The absorption of NIR photons not only can generate extra photocurrent for the solar cell but also can reduce the amount of heat passing through the device. A dual-function ultrathin Ag film was applied as the top transparent electrode for charge collection as well as an IR reflector to block out a significant amount of heat. To further enhance the optical and heat-rejection properties of the ST-OPV, we further introduced a four-layer DBR structure on top of the Ag film to selectively reflect the NIR light while maintaining good transparency for the visible wavelengths to maximize the heat insulation without sacrificing the optical and power-generation properties of the ST-OPV. As a result, through these synergic material and optical engineering strategies, we have demonstrated a value-added ST-OPV with PCE of 6.5% and AVT of 25% in addition to an excellent IR radiation rejection rate of over 80%, which paves the way for the new application of OPV technology for both power generation and power saving.

RESULTS AND DISCUSSION

A blend of commercially available low-bandgap semiconductors was used in the device, with a configuration of indium tin oxide (ITO)/PEDOT:PSS/PBDTTT-E-T:IEICO/interlayer/Ag. The molecular structures of the donor and acceptor, which have proved to be promising candidates as the active-layer materials for non-fullerene OPVs,[31] are presented in Figure S1A. Another reason to choose the

[1]Institute of Polymer Optoelectronic Materials and Devices, State Key Laboratory of Luminescent Materials and Devices, South China University of Technology, Guangzhou 510640, P.R. China

[2]State Key Laboratory of Polymer Physics and Chemistry, Beijing National Laboratory for Molecular Sciences, Institute of Chemistry, Chinese Academy of Sciences, Beijing 100190, P.R. China

[3]Innovation Center for Printed Photovoltaics, South China Institute of Collaborative Innovation, Dongguan 523808, P.R. China

[4]These authors contributed equally

[5]Lead Contact

*Correspondence: msfhuang@scut.edu.cn (F.H.), msangusyip@scut.edu.cn (H.-L.Y.)

https://doi.org/10.1016/j.joule.2018.06.006

Please cite this article in press as: Sun et al., Heat-Insulating Multifunctional Semitransparent Polymer Solar Cells, Joule (2018), https://doi.org/10.1016/j.joule.2018.06.006

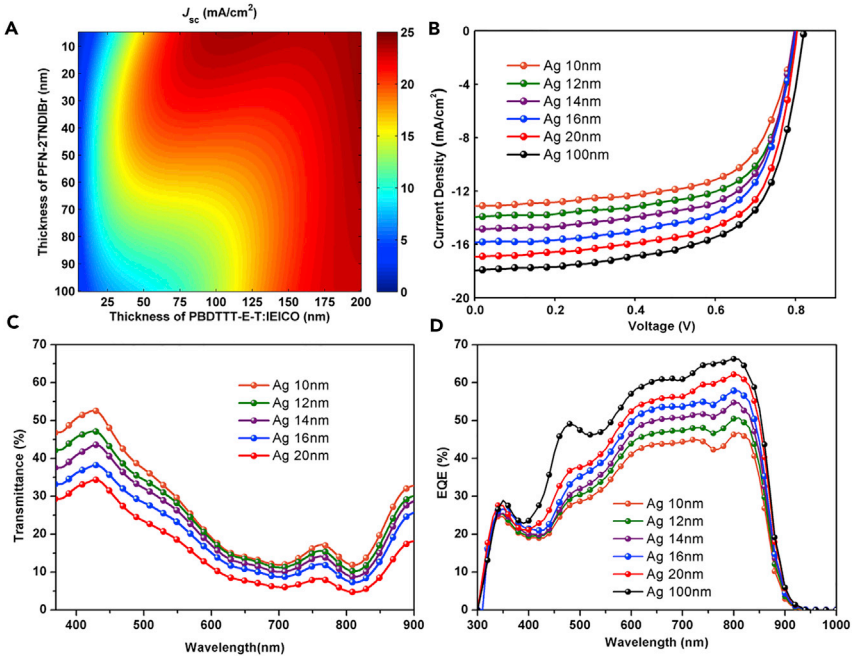

Figure 1. Simulated Data and Experimental Characteristics

(A) Simulated $J_{sc\ (IQE=100\%)}$ generated in ST-OPVs as a function of active layer and interlayer thickness.

(B) Typical *J-V* characteristics.

(C) Transmission spectra.

(D) External quantum efficiency (EQE) spectra of semitransparent and opaque devices with various Ag thicknesses.

PBDTTT-E-T:IEICO blend for this study is its relatively weak absorption in the visible range (as shown in Figure S1B), which is favorable for improving the AVT of the ST-OPVs. An n-type conjugated polyelectrolyte, PFN-2TNDI-Br, was chosen as the interlayer material because it is a self-doped polymer with enhanced electron-transporting capability[32]; it can also provide an extra interface for charge dissociation in non-fullerene solar cells[33] and suitable surface properties to promote the growth of high-quality ultrathin metal film transparent electrode for ST-OPVs.[34] The ST-OPVs were fabricated with the same device architecture as the opaque cells except an ultrathin semitransparent Ag electrode with thickness between 10 and 20 nm was applied as the top transparent electrode. To study the initial performance of the ST-OPVs, we chose a Ag top transparent electrode of thickness 16 nm. We then used a transfer matrix model to provide guidelines for the optimal thickness of the active layer and interlayer in the ST-OPVs. According to the simulation result shown in Figure 1A, there are two regions that can achieve high photocurrents. One is located at the region where the active-layer thickness is between 80 and 140 nm and the interlayer thickness is small (<20 nm); it is worth noting that within this region the optimal short-circuit current density (J_{sc}) shifts toward the thinner active-layer thickness when the interlayer thickness increases. The second high-photocurrent region can be achieved at larger active-layer film thickness (~200 nm) regardless of the interlayer thickness. As it is known that recombination could be severed and limits the performance of non-fullerene OPVs when the active layer is thick, here we chose to focus our study on the devices with thinner active-layer films. A series of devices with selected structures comprising different component-layer thicknesses within the optimized thickness matrix were fabricated, and the device results are

Please cite this article in press as: Sun et al., Heat-Insulating Multifunctional Semitransparent Polymer Solar Cells, Joule (2018), https://doi.org/10.1016/j.joule.2018.06.006

Table 1. Photovoltaic Parameters of Solar Cells with Various Ag Thicknesses under the Same Optimized Conditions

Ag Thickness (nm)	V_{oc} (V)	J_{sc} (mA/cm^2)	FF	PCE (%)	PCE_{max} (%)
10	0.81 ± 0.01	12.6 ± 0.5	0.65 ± 0.01	6.4 ± 0.4	6.8
12	0.81 ± 0.01	13.5 ± 0.5	0.66 ± 0.01	7.1 ± 0.3	7.4
14	0.81 ± 0.01	14.4 ± 0.4	0.66 ± 0.01	7.7 ± 0.2	7.9
16	0.81 ± 0.01	15.4 ± 0.5	0.66 ± 0.01	8.2 ± 0.2	8.4
20	0.81 ± 0.01	16.3 ± 0.3	0.67 ± 0.01	8.7 ± 0.3	9.0
100	0.81 ± 0.01	17.6 ± 0.4	0.67 ± 0.01	9.4 ± 0.3	9.7

summarized in Table S1. When the thickness of the active layer increased from 80 to 137 nm, the performance of the devices with each interlayer thickness (5, 11, and 17 nm) did not change significantly, in good agreement with the optical modeling results. Among the three different interlayer thicknesses, the ST-OPVs with interlayer thickness of 11 nm showed generally higher performance than those with other interlayer thicknesses. The results could be attributed to both the optical spacer effect and additional charge-generation effect at the bulk heterojunction/interlayer interface, which had been discussed previously in another report.[33] The best performance of the studied devices was obtained with the active-layer and interlayer thickness of 80 nm and 11 nm, respectively, producing an ST-OPV with a PCE of 8.4%, a J_{sc} of 15.5 mA/cm^2, a V_{oc} of 0.81 V, and a fill factor (FF) of 0.67. Therefore, in the following study we chose to fix these layer thicknesses and continue the optimization of the performance of the ST-OPVs by varying the thicknesses of the top transparent electrode.

To evaluate the relationship between AVT and PCE of the ST-OPVs, we obtained a gradient change of the transmittance of the cells by linearly increasing the thickness of the top Ag electrode from 10 to 20 nm while keeping the other layers at the optimal thickness described above. An additional opaque cell based on a 100-nm Ag mirror top electrode was also fabricated as reference. The current density-voltage (*J-V*) curves, transmittance curves, and external quantum efficiency (EQE) of these ST-OPVs with different electrode thicknesses are shown in Figures 1B–1D, respectively. The solar cell parameters and the AVT (calculated from 380 to 780 nm) of the corresponding devices are summarized in Table 1. The reference opaque cell showed promising performance with a PCE of 9.7% and a J_{sc} of 17.7 mA/cm^2. When the thickness of the top electrode is gradually reduced, the J_{sc} decreases and AVT increases because the thinner silver film reflects less light back to the light-harvesting layer and transmits more light through the device. As a result, the PCE of the ST-OPVs increases with Ag thickness as the J_{sc} increases (Figure 1B) while a corresponding decrease of AVT is observed (Figure 1C). It is worth noting that for the ST-OPV cell with 20 nm Ag, the J_{sc} value is more than 90% of that of the opaque cell. Even with Ag thickness reduced down to 10 nm, the J_{sc} still maintains over 70% of the original J_{sc}; these values are indeed very high for ST-OPVs. The trend of the transmittance loss upon increasing Ag thickness as shown in Figure 1B correlates well with the simulated transmittance curves (Figure S2), which suggests that the optical model can be a very useful tool to predict the optical properties of ST-OPVs. Experimental EQE curves for the semitransparent and opaque cells are shown in Figure 1D. The trend observed is in good agreement with the change of the J_{sc} values, with a gradual decrease in EQE across the whole spectrum when the Ag thickness decreases.

The PCE versus AVT for the ST-OPVs are further plotted in Figure S3; in addition, a previously reported ST-OPV performance[5] based on the blend of $PC_{71}BM$ and a

Please cite this article in press as: Sun et al., Heat-Insulating Multifunctional Semitransparent Polymer Solar Cells, Joule (2018), https://doi.org/10.1016/j.joule.2018.06.006

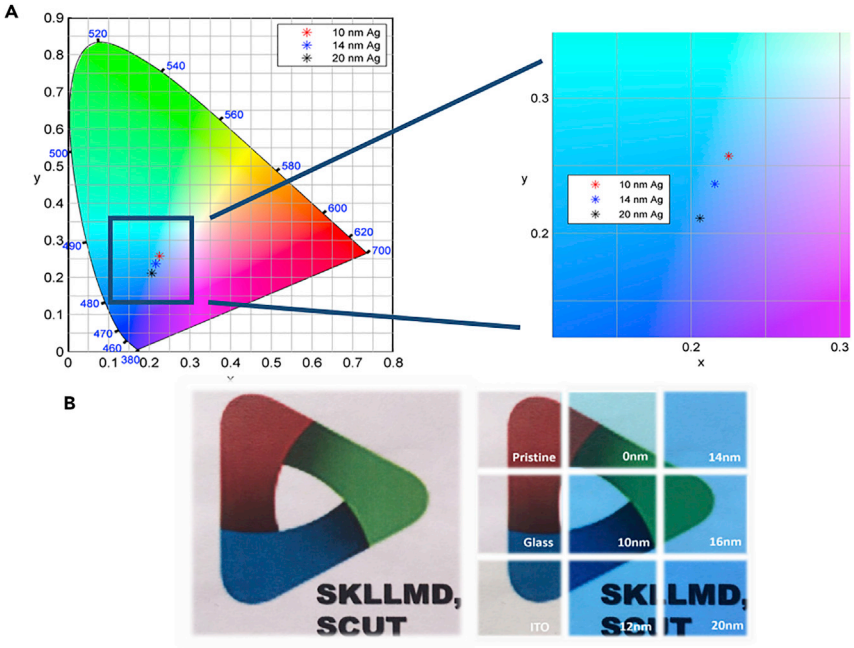

Figure 2. Transparency Color Properties

(A) Representation of the ST-OPV color coordinates with different Ag thicknesses, on a CIE 1931xyY chromaticity diagram.

(B) Digital photographs taken through the semitransparent devices, demonstrating color and transparency.

similar polymer with the same conjugated backbone used in this study is also plotted for comparison. The results show that the PCE is linearly dependent on the AVT with PCE between 6.8% and 9% and the corresponding AVT between 28% and 17%. In addition, the performance of the small-bandgap non-fullerene acceptor (NFA)-based ST-OPVs are much better than the fullerene-based ST-OPVs. For example, at a similar AVT of ~20%, the former ST-OPV delivers a PCE of 8.4% while the latter only shows a PCE of 6.2%. A significant contribution to this enhanced performance is from the IR light-harvesting property of the non-fullerene acceptor, which generates extra photocurrent from the NIR photons without losing much on the visible transmittance. The EQE spectra in Figure 1D clearly show that the major portion of the photocurrent is generated at the NIR region, while the visible region, particularly from 380 to 600 nm, contributes relatively small photocurrent. This outcome is reflected on the transmittance spectra shown in Figure 1C, showing a much higher transmittance at the visible range, which is favorable for ST-OPVs. These results suggest that the unique optical property of small-bandgap non-fullerene acceptors with localized absorption in the NIR makes them a perfect material choice for ST-OPVs.

The color properties of the resulting ST-OPVs are further discussed here, as both the esthetic consideration and human color perception are very important factors in building window applications. The perceived transparency of ST-OPVs by human eyes plays a significant role in evaluating the overall color-rendering property for the devices.[35,36] The color coordinates (x, y) were calculated from the transmission spectrum of ST-OPVs, which is specifically designed to represent human visual color perception. The color coordinates of our ST-OPVs with different Ag thicknesses in the CIE 1931 chromaticity diagram are illustrated in Figure 2A. We chose three representative thicknesses for electrodes, which could cover the range of thickness

Please cite this article in press as: Sun et al., Heat-Insulating Multifunctional Semitransparent Polymer Solar Cells, Joule (2018), https://doi.org/10.1016/j.joule.2018.06.006

we used in our ST-OPVs. The corresponding coordinates of the devices derived from 10-, 14-, and 20-nm Ag cathodes are (0.225, 0.257), (0.215, 0.236), and (0.205, 0.211), respectively, with the correlated color temperature and general color-rendering index of the devices shown in Table S3. In addition, digital photographs were taken through an array of ST-OPVs with various transparencies as shown in Figure 2B. All of the semitransparent devices showed a very nice transparency color perception that appeared as bluish. These photos also show that the ST-OPVs demonstrate not only excellent visible light transparency but also an appealing color appearance that is important for architectural design.

In addition to their excellent device performance and appealing appearance, potentially ST-OPVs can also serve as efficient heat-insulating window films provided they can adequately absorb or reflect the sun's energy and reduce the solar heat transmitted through the ST-OPV to the interior of building. The sun radiates solar energy by photons with wavelengths covered from 290 to 2,500 nm, which can be further divided into three bands including UV (290–380 nm), visible (380–780 nm), and IR light (780–2,500 nm) (https://www.icnirp.org/). The energy distribution within the solar spectrum is approximately 3%, 44%, and 53% for the UV, visible, and IR light, respectively. An ideal solar window film should block out all the UV and IR light while allowing most of the visible light passing through to provide a good heat-rejection effect and high visible transmittance. In the case of ST-OPVs, since most organic semiconductors have strong absorption for visible light, inevitably the visible light-harvesting and transmission properties have to be balanced to achieve both good PCE and transparency, while both UV and IR light should still be absorbed or reflected by the ST-OPV to maintain the good heat-insulation function. Therefore, in this study, in addition to the PCE and AVT of the ST-OPVs, we also evaluate their performance based on the IR radiation rejection properties and compare them with some state-of-the-art commercial solar films.

In our ST-OPV design, the solar light enters through the ITO side and a portion of the visible and NIR will be absorbed by the light-harvesting layer before encountering the thin Ag transparent electrode. As the ultrathin Ag film is a relatively good transmitter for visible light but a good mirror for IR light, a portion of the visible light will transmit through the ST-OPV but most IR light will be reflected back.[37] As shown in Figure S4, when the transmission spectrum of the ST-OPVs were tested to 2,500 nm, the transmittance decreased rapidly as the Ag thickness increased, particularly at the region with wavelengths larger than 1,500 nm. This heat-mirror effect of Ag electrodes also helps to reflect some NIR light back to the light-harvesting layer, which eventually is absorbed and converted to photocurrent as shown in the 780- to 900-nm region of the EQE spectrum in Figure 1D.

The advantage of the proposed heat-insulation function for our ST-OPVs is clearly illustrated in Table 2, in which we compare the AVT (from 380 to 780 nm) and IR radiation rejection (from 780 to 2,500 nm) properties of our ST-OPVs with three different kinds of commercially available solar films produced by the 3M company. The optical data were measured directly using a commercial solar-film transmission meter. When the Ag thickness of the ST-OPVs increased from 10 to 20 nm, the IR rejection increased from 75% to 90% with a corresponding drop of AVT from 25.1% to 17.7%. These visible transmission and heat-insulation properties are indeed very comparable with some of the commercial films. For example, the ST-OPVs with 10 and 20 nm Ag showed comparable transmittance and heat rejection with the NV-25 and P-18ARL solar films, respectively, but in addition these ST-OPVs can also generate power under solar radiation with corresponding PCEs of

Please cite this article in press as: Sun et al., Heat-Insulating Multifunctional Semitransparent Polymer Solar Cells, Joule (2018), https://doi.org/10.1016/j.joule.2018.06.006

Table 2. Visible Transmittance and Heat Rejection for Commercial Solar Films and ST-OPVs with Various Electrode Thicknesses

	Average Visible Light Transmittance (%)	Infrared Radiation Rejection (%)
10 nm Ag	25.1	75.0
12 nm Ag	24.0	78.3
14 nm Ag	23.8	81.0
16 nm Ag	22.8	83.1
20 nm Ag	17.7	90.0
3M P-18ARL	15.9	90.9
3M NV-25	26.4	69.7
3M PR70	67.5	91.6

6.8% and 9% (as shown in Table 1). Taking one step further, to evaluate the actual capability of the ST-OPVs for reducing temperature under illumination we used a Philips infrared lamp to heat the metal object through a glass substrate or an ST-OPV device, and took thermal images of the metal with an IR camera. As shown in Figure 3, after illumination the temperature of the object reached approximately 35°C with a glass filter, while it remained below 31°C with the ST-OPV, which possesses an IR-rejection rate of 75%. These results illustrate that the proposed ST-OPVs can effectively reduce the solar heat flux and can potentially be used as a power-generating and heat-control window to provide electricity and also keep the interior of the building or automobile cool.

For the three commercial solar films we chose, the PR70 solar film shows the most ideal properties with both high AVT and IR-rejection rate. Different from the two other solar films, which are based on a reflective metal coating to enhance IR rejection, the PR70 film utilizes a sophisticated photonic crystal design with alternating thin films of high- and low-refractive index materials,[38–41] forming a DBR that can selectively reflect a major portion of IR light while keeping a high visible light transmittance. Although it is unrealistic for ST-OPVs to possess such a high AVT as they need to harvest a good amount of visible light to generate power, it is possible to introduce a simple DBR to the ST-OPV to further enhance the IR reflection in the devices. Such a concept is presented in Figure 4A. Guided by optical simulations, a periodic LiF/MoO_3 multilayer DBR with optimized structure was introduced to obtain maximum reflectivity for the NIR light to further improve heat rejection at the DBR/Ag interface while maintaining good visible transmittance (as shown in Figure 4B). The DBR was deposited by thermal evaporation that imposed no degradation on the performance of the solar cells. After adding the DBR, the ST-OPV (device B) showed a more effective NIR photon reflection, leading to an increased IR-rejection rate from 75% to 80%, while the transparency in the visible region was maintained close to 25%, which is in good agreement with the prediction from the optical simulation. Accordingly, the efficiency of device B with DBR was still maintained at over 6.5%, as shown in Table S4 and Figure S5. Further improvement in the IR absorption of active layers, minimization of parasitic losses, and development of appropriate photonic crystals could further improve the device performance and IR-rejection property of ST-OPVs.

Finally, we further demonstrated that the dual-functional ST-OPVs can also be fabricated on thin plastic substrate with good form factor comparable with the current commercial solar films. As shown in Figure S7, flexible ST-OPVs were fabricated

Please cite this article in press as: Sun et al., Heat-Insulating Multifunctional Semitransparent Polymer Solar Cells, Joule (2018), https://doi.org/10.1016/j.joule.2018.06.006

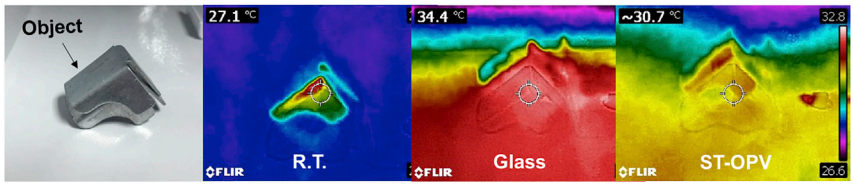

Figure 3. Thermal Images Taken with an IR Camera for Comparing Heat-Rejection Properties

on polyethylene naphthalate (PEN)/ITO substrates (sheet resistance of 20 Ω^{-1}), and the device performances are summarized in Table S5. Compared with glass/ITO-based ST-OPVs, the PEN-based flexible devices exhibited a reduced FF value due to the larger sheet resistance and reduced transmittance of the PEN/ITO substrates; however, the average PCE was still maintained at 6% with AVT of 23%. The demonstration of flexible ST-OPVs further opens up a new opportunity for their integration with windows on buildings. They can now be easily pasted on existing building windows or even can be made as a solar curtain that can generate power and also provide heat control.

In summary, we have developed high-performance semitransparent organic solar cells that can be used for power-generating and heat-insulating window films. The use of non-fullerene acceptor with enhanced absorption in the NIR region enables the harvesting of NIR light, resulting in ST-OPVs with high PCE and AVT. In addition, the effectiveness in blocking IR light endows the semitransparent device with excellent heat-insulation properties that already meet the commercial requirements. By further optimizing the optical design of the ST-OPVs using a tailored DBR, we demonstrated even better heat rejection of the ST-OPVs while maintaining similar visible light transparency and photovoltaic performance. The novel design concept presented in this work is expected to open up a new approach to developing multifunctional yet efficient semitransparent organic solar cells, which can greatly enhance their integration into various future applications.

EXPERIMENTAL PROCEDURES

Materials

PFN-2TNDI-Br were synthesized according to the reported procedure.[32] PBDTTT-E-T and IEICO were purchased from Solarmer Materials. Unless otherwise stated, all reagents and solvents were commercially available products and were used as received.

ST-OPV Device Fabrication

The ITO glass (sheet resistance of 11 Ω^{-1}) and PEN substrates were cleaned using a standard procedure. A PEDOT:PSS layer (~20 nm) was spun on an ITO substrate and dried at 140°C for 20 min in air. PBDTTT-E-T:IEICO (1:1 weight ratio) in chlorobenzene:DIO (98:2 volume ratio) solution were spin-coated to obtain films with different thickness. Preparation of the blend solutions and subsequent spin coating and annealing onto the PEDOT:PSS films were carried out in a N_2-filled glovebox. The PFN-2TNDI-Br dissolved in methanol at a concentration of 0.5–1 mg/mL was spun onto the active layers at 2,000 rpm for 30 s for different thickness devices. A silver electrode was deposited by thermal evaporation finally through a shadow mask under a base pressure of 1×10^{-7} mbar, which defines the active cell area of 0.05 cm^2. To improve the accuracy of measurement, we put a non-refractive mask with an aperture of 0.04 cm^2 in close contact and aligned it with the solar cells, which defines the illumination area to be 0.04 cm^2.

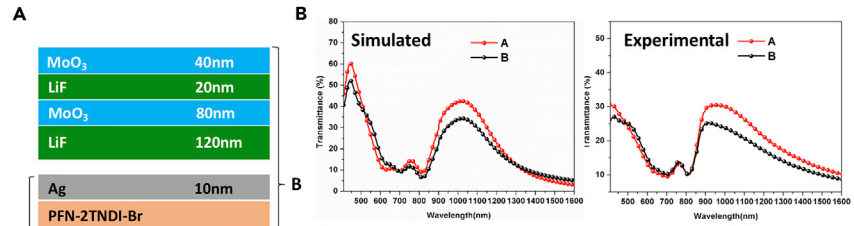

Device	Visible Light Transmittance (%)	Infrared Radiation Rejection (%)
A	25.1	75.6
B	26.2	80.6

Figure 4. Interference Optimization

(A) Schematic view of the fabricated ST-OPV (device A) and ST-OPV with Bragg reflectors (device B).

(B) The simulated and experimental transmission spectra for the ST-OPVs with or without distributed Bragg reflectors.

(C) The visible transmittance and heat rejection of device A and device B.

Device Characterization

The device photocurrent was measured under an AM 1.5G solar simulator (Enlitech, Taiwan). The current density-voltage (*J-V*) characteristics for the devices were recorded with a Keithley 2400 source meter, and no applied bias or light soaking process was applied before *J-V* measurement. The illumination intensity of the light source was calibrated with a reference monocrystal silicon cell (Enlitech) calibrated by China General Certification Center, giving a value of 100 mW/cm^2 in the test. The EQE study was performed on a commercial EQE measurement system (QE-R3011; Enlitech). The thickness was obtained from surface profiler measurements, in combination with extrapolation from an absorbance thickness curve that assumed a linear dependence of absorbance for PFN-2TNDI-Br on the film thickness. The heat-insulating parameters in Table 2 and thermal images were recorded on a commercial solar-film transmission meter (LS182; Linshang) and an infrared camera (FLIR C2), respectively.

Optical Modeling

Optical modeling was based on the Transfer Matrix Formalism. The optical parameters of n (refractive index) and k (extinction coefficient) for different films were measured using a dual rotating-compensator Mueller matrix ellipsometer (ME-L; Wuhan Eoptics Technology, Wuhan, China). A more detailed description for the optical parameters can be found in Zhang et al.[42] For the evaluation of the color-rendering indices, the experimental transmission of each device is folded with the AM1.5 spectrum to obtain the perceived transmission under solar illumination. The resulting data are coupled with the CIE 1931 2° standard observer color-matching functions to obtain the corresponding xyY points.

SUPPLEMENTAL INFORMATION

Supplemental Information includes eight figures and five tables and can be found with this article online at https://doi.org/10.1016/j.joule.2018.06.006.

ACKNOWLEDGMENTS

The work was financially supported by the Natural Science Foundation of China (nos. 91633301, 21761132001, and 51573057), the Ministry of Science and Technology

(nos. 2014CB643505 and 2017YF0206600), and the Science and Technology Program of Guangzhou, China (nos. 201607020010 and 2017A050503002).

AUTHOR CONTRIBUTIONS

H.-L.Y. proposed the research, directed the study, and analyzed the data. C.S. carried out the device fabrication and characterizations. R.X. built the optical model and participated in the discussion. X.L. prepared active layer and interlayer materials for device fabrication. H.S. helped with the solar cell fabrication. H.Y. and J.H. provided the solar cell materials. H.-L.Y. and C.S. prepared the manuscript. Y.C., F.H., and H.-L.Y. supervised the whole project. All authors discussed the results and commented on the manuscript.

DECLARATION OF INTERESTS

The authors declare no competing interests.

Received: April 25, 2018
Revised: May 22, 2018
Accepted: June 5, 2018
Published: July 3, 2018

REFERENCES

1. Krebs, F.C., Espinosa, N., Hösel, M., Søndergaard, R.R., and Jørgensen, M. (2014). 25th anniversary article: rise to power—OPV-based solar parks. Adv. Mater. *26*, 29–39.

2. Li, G., Zhu, R., and Yang, Y. (2012). Polymer solar cells. Nat. Photonics *6*, 153–161.

3. Yu, G., Gao, J., Hummelen, J.C., Wudl, F., and Heeger, A.J. (1995). Polymer photovoltiac cells: enhanced efficiencies via a network of internal donor-acceptor heterojunctions. Science *270*, 1789–1791.

4. Halls, J.J.M., Walsh, C.A., Greenham, N.C., Marseglia, E.A., Friend, R.H., Moratti, S.C., and Holmes, A.B. (1995). Efficient photodiodes from interpenetrating polymer networks. Nature *376*, 498–500.

5. Chen, K.-S., Salinas, J.-F., Yip, H.-L., Huo, L., Hou, J., and Jen, A.K.Y. (2012). Semi-transparent polymer solar cells with 6% PCE, 25% average visible transmittance and a color rendering index close to 100 for power generating window applications. Energy Environ. Sci. *5*, 9551–9557.

6. Guo, F., Zhu, X., Forberich, K., Krantz, J., Stubhan, T., Salinas, M., Halik, M., Spallek, S., Butz, B., Spiecker, E., et al. (2013). ITO-free and fully solution-processed semitransparent organic solar cells with high fill factors. Adv. Energy Mater. *3*, 1062–1067.

7. Xue, Q., Xia, R., Brabec, C.J., and Yip, H.-L. (2018). Recent advances in semi-transparent polymer and perovskite solar cells for power generating window applications. Energy Environ. Sci. https://doi.org/10.1039/C1038EE00154E.

8. Chan, W.W., Mak, L.M., Chen, Y.M., Wang, Y.H., Xie, H.R., Hou, G.Q., and Li, D. (2008). Energy saving and tourism sustainability: solar control window film in hotel rooms. J. Sustain. Tourism *16*, 563–574.

9. Li, C., Tan, J., Chow, T.-T., and Qiu, Z. (2015). Experimental and theoretical study on the effect of window films on building energy consumption. Energy Build. *102*, 129–138.

10. Kaklauskas, A., Zavadskas, E.K., Raslanas, S., Ginevicius, R., Komka, A., and Malinauskas, P. (2006). Selection of low-e windows in retrofit of public buildings by applying multiple criteria method COPRAS: a Lithuanian case. Energy Build. *38*, 454–462.

11. Cuce, E., Young, C.-H., and Riffat, S.B. (2014). Performance investigation of heat insulation solar glass for low-carbon buildings. Energy Convers. Manag. *88*, 834–841.

12. Young, C.-H., Chen, Y.-L., and Chen, P.-C. (2014). Heat insulation solar glass and application on energy efficiency buildings. Energy Build. *78*, 66–78.

13. Ando, E., Suzuki, S., Aomine, N., Miyazaki, M., and Tada, M. (2000). Sputtered silver-based low-emissivity coatings with high moisture durability. Vacuum *59*, 792–799.

14. Betancur, R., Romero-Gomez, P., Martinez-Otero, A., Elias, X., Maymo, M., and Martorell, J. (2013). Transparent polymer solar cells employing a layered light-trapping architecture. Nat. Photonics *7*, 995–1000.

15. Quiroz, C.O.R., Levchuk, I., Bronnbauer, C., Salvador, M., Forberich, K., Heumuller, T., Hou, Y., Schweizer, P., Spiecker, E., and Brabec, C.J. (2015). Pushing efficiency limits for semitransparent perovskite solar cells. J. Mater. Chem. A *3*, 24071–24081.

16. Tang, Z., George, Z., Ma, Z., Bergqvist, J., Tvingstedt, K., Vandewal, K., Wang, E., Andersson, L.M., Andersson, M.R., Zhang, F., and Inganäs, O. (2012). Semi-transparent tandem organic solar cells with 90% internal quantum efficiency. Adv. Energy Mater. *2*, 1467–1476.

17. Schmidt, H., Flügge, H., Winkler, T., Bülow, T., Riedl, T., and Kowalsky, W. (2009). Efficient semitransparent inverted organic solar cells with indium tin oxide top electrode. Appl. Phys. Lett. *94*, 163.

18. Chang, C.-Y., Zuo, L., Yip, H.-L., Li, C.-Z., Li, Y., Hsu, C.-S., Cheng, Y.-J., Chen, H., and Jen, A.K.Y. (2014). Highly efficient polymer tandem cells and semitransparent cells for solar energy. Adv. Energy Mater. *4*, 1301645.

19. Min, J., Bronnbauer, C., Zhang, Z.-G., Cui, C., Luponosov, Y.N., Ata, I., Schweizer, P., Przybilla, T., Guo, F., Ameri, T., et al. (2016). Fully solution-processed small molecule semitransparent solar cells: optimization of transparent cathode architecture and four absorbing layers. Adv. Funct. Mater. *26*, 4543–4550.

20. Yusoff, A.R.b. M., Lee, S.J., Shneider, F.K., da Silva, W.J., and Jang, J. (2014). High-performance semitransparent tandem solar cell of 8.02% conversion efficiency with solution-processed graphene mesh and laminated Ag nanowire top electrodes. Adv. Energy Mater. *4*, 1301989.

21. Chen, C.-C., Dou, L., Zhu, R., Chung, C.-H., Song, T.-B., Zheng, Y.B., Hawks, S., Li, G., Weiss, P.S., and Yang, Y. (2012). Visibly transparent polymer solar cells produced by solution processing. ACS Nano *6*, 7185–7190.

22. Dou, L., Chang, W.-H., Gao, J., Chen, C.-C., You, J., and Yang, Y. (2013). A selenium-substituted low-bandgap polymer with versatile photovoltaic applications. Adv. Mater. *25*, 825–831.

23. Zhao, F., Dai, S., Wu, Y., Zhang, Q., Wang, J., Jiang, L., Ling, Q., Wei, Z., Ma, W., You, W., et al. (2017). Single-junction binary-blend nonfullerene polymer solar cells with 12.1% efficiency. Adv. Mater. *29*, 1700144.

24. Bin, H., Gao, L., Zhang, Z.-G., Yang, Y., Zhang, Y., Zhang, C., Chen, S., Xue, L., Yang, C., Xiao, M., and Li, Y. (2016). 11.4% Efficiency non-fullerene polymer solar cells with trialkylsilyl substituted 2D-conjugated polymer as donor. Nat. Commun. *7*, 13651.

25. Liu, F., Zhou, Z., Zhang, C., Zhang, J., Hu, Q., Vergote, T., Liu, F., Russell, T.P., and Zhu, X. (2017). Efficient semitransparent solar cells with high NIR responsiveness enabled by a small-bandgap electron acceptor. Adv. Mater. *29*, https://doi.org/10.1002/adma.201606574.

26. Upama, M.B., Wright, M., Elumalai, N.K., Mahmud, M.A., Wang, D., Xu, C., and Uddin, A. (2017). High-efficiency semitransparent organic solar cells with non-fullerene acceptor for window application. ACS Photonics *4*, 2327–2334.

27. Jia, B., Dai, S., Ke, Z., Yan, C., Ma, W., and Zhan, X. (2018). Breaking 10% efficiency in semitransparent solar cells with fused-undecacyclic electron acceptor. Chem. Mater. *30*, 239–245.

28. Li, Y., Lin, J.-D., Che, X., Qu, Y., Liu, F., Liao, L.-S., and Forrest, S.R. (2017). High efficiency near-infrared and semitransparent non-fullerene acceptor organic photovoltaic cells. J. Am. Chem. Soc. *139*, 17114–17119.

29. Li, Y., Zhong, L., Gautam, B., Bin, H.-J., Lin, J.-D., Wu, F.-P., Zhang, Z., Jiang, Z.-Q., Zhang, Z.-G., Gundogdu, K., et al. (2017). A near-infrared non-fullerene electron acceptor for high performance polymer solar cells. Energ Environ. Sci. *10*, 1610–1620.

30. Wang, W., Yan, C., Lau, T.K., Wang, J., Liu, K., Fan, Y., Lu, X., and Zhan, X. (2017). Fused hexacyclic nonfullerene acceptor with strong near-infrared absorption for semitransparent organic solar cells with 9.77% efficiency. Adv. Mater. *29*, 1701308.

31. Yao, H., Chen, Y., Qin, Y., Yu, R., Cui, Y., Yang, B., Li, S., Zhang, K., and Hou, J. (2016). Design and synthesis of a low bandgap small molecule acceptor for efficient polymer solar cells. Adv. Mater. *28*, 8283–8287.

32. Wu, Z., Sun, C., Dong, S., Jiang, X.-F., Wu, S., Wu, H., Yip, H.-L., Huang, F., and Cao, Y. (2016). n-Type water/alcohol-soluble naphthalene diimide-based conjugated polymers for high-performance polymer solar cells. J. Am. Chem. Soc. *138*, 2004–2013.

33. Sun, C., Wu, Z., Hu, Z., Xiao, J., Zhao, W., Li, H.-W., Li, Q.-Y., Tsang, S.-W., Xu, Y.-X., Zhang, K., et al. (2017). Interface design for high-efficiency non-fullerene polymer solar cells. Energy Environ. Sci. *10*, 1784–1791.

34. Shi, H., Xia, R., Sun, C., Xiao, J., Wu, Z., Huang, F., Yip, H.L., and Cao, Y. (2017). Synergic interface and optical engineering for high-performance semitransparent polymer solar cells. Adv. Energy Mater. *7*, 1701121.

35. Chang, S.-Y., Cheng, P., Li, G., and Yang, Y. (2018). Transparent polymer photovoltaics for solar energy harvesting and beyond. Joule. https://doi.org/10.1016/j.joule.2018.1004.1005.

36. Yaowen, L., Guiying, X., Chaohua, C., and Yongfang, L. (2018). Flexible and semitransparent organic solar cells. Adv. Energy Mater. *8*, 1701791.

37. Kim, H., Kim, H.-S., Ha, J., Park, N.-G., and Yoo, S. (2016). Empowering semi-transparent solar cells with thermal-mirror functionality. Adv. Energy Mater. *6*, 1502466.

38. Yu, W., Jia, X., Yao, M., Zhu, L., Long, Y., and Shen, L. (2015). Semitransparent polymer solar cells with simultaneously improved efficiency and color rendering index. Phys. Chem. Chem. Phys. *17*, 23732–23740.

39. Yu, W., Shen, L., Jia, X., Liu, Y., Guo, W., and Ruan, S. (2015). Improved color rendering index of low band gap semi-transparent polymer solar cells using one-dimensional photonic crystals. RSC Adv. *5*, 54638–54644.

40. Shen, P., Wang, G., Kang, B., Guo, W., and Shen, L. (2018). High-efficiency and high-color-rendering-index semitransparent polymer solar cells induced by photonic crystals and surface plasmon resonance. ACS Appl. Mater. Interfaces *10*, 6513–6520.

41. Xu, G., Shen, L., Cui, C., Wen, S., Xue, R., Chen, W., Chen, H., Zhang, J., Li, H., Li, Y., and Li, Y. (2017). High-performance colorful semitransparent polymer solar cells with ultrathin hybrid-metal electrodes and fine-tuned dielectric mirrors. Adv. Funct. Mater. *27*, 1605908.

42. Zhang, K., Gao, K., Xia, R., Wu, Z., Sun, C., Cao, J., Qian, L., Li, W., Liu, S., Huang, F., et al. (2016). High-performance polymer tandem solar cells employing a new n-type conjugated polymer as an interconnecting layer. Adv. Mater. *28*, 4817–4823.